JOURNAL OF MATERIALS SCIENCE 32 (1997) 5513–5524

Textural evolution in electrodeposits under the influence of adsorbed foreign species

Part I *Textural evolution in iron electrodeposits affected by hydrogen co-deposition*

D. Y. LI
Department of Materials Science and Engineering, The Pennsylvania State University, University Park, PA 16802, USA

J. A. SZPUNAR
Department of Metallurgical Engineering, McGill University, 3450 University Street, Montreal, PQ, Canada H3A 2A7

Textural evolution in electrodeposits is strongly affected by foreign species in the electrolyte and also by the co-deposition of hydrogen. The effects of foreign species on textural development in electrodeposits were studied by employing a Monte Carlo model. This model is based on physical principles and incorporates parameters which are used to control electrodeposition processes. An attempt was made in the simulation to reflect the basic process of the deposit growth, and to identify the factors responsible for the texture formation and its variation with the deposition condition. It is assumed that the texture of the deposit results from the minimization of the free energy of the system. Based on this assumption, it was demonstrated that the surface-energy anisotropy played an important role in the formation of fibre texture. In particular, the model can be used to simulate textural evolution under the influence of adsorbed foreign species, because the surface-energy anisotropy is modified by the adsorbed foreign species. Part I of the paper presents results of our studies on iron electrodeposition with the emphasis on the effect of hydrogen adsorption on iron deposit texture. Relevant experimental results have also been presented to corroborate the simulation study. Part II of the paper presents simulation studies of textural evolution in copper deposits under the influence of adsorbed potassium and chloride ions.

1. Introduction

The texture of electrodeposits is strongly affected by the deposition condition and is particularly sensitive to foreign species generally existing in the electrolyte. During electrodeposition, foreign species may be co-deposited or adsorbed by the deposit, resulting in changes in the deposit texture. In addition, evolved hydrogen may also cause changes in texture. However, how the adsorbed foreign species cause textural variation is unclear, because the mechanism of texture formation during electrodeposition is not well understood. Several theories were developed to explain the texture formation during electrodeposition [1–6]. These theories fall into two categories: one is called the geometrical selection theory [1], which suggests that the texture formation is attributed to the difference in the advance rate between different planes, and also attributed to the deposit surface morphology. According to this theory, there are two modes for deposit growth: the outward growth mode and the lateral growth mode. In the outward growth mode, the grains bounded by slow-growing faces (i.e. close-packed faces), which are perpendicular to the substrate, grow preferentially, whereas in the lateral growth mode, the grains bounded by slow-growing faces, which are parallel to the substrate, grow preferentially. Different growth modes result in different textures. This theory, however, cannot answer the question of what determines the crystal growth mode, and disagreement between this theory and experiments exists.

Another theory, called the two-dimensional nucleation theory [2, 7], assumes that the nucleation rate of two-dimensional nuclei formed on the deposit surface is the factor determining the texture of the deposit. The theory suggests that the nucleation rate can be expressed as $\exp(-W_{hkl}/KT)$: W_{hkl} is the nucleation energy, which corresponds to the overpotential, and is dependent upon the orientation of the crystal plane on which the nucleus forms, as well as upon the orientation of the nucleus. According to this theory,

0022–2461

differently oriented crystal planes have different overpotentials, and this causes different nucleation rates, leading to a textured electrodeposit. However, the operating overpotential for metal deposition is generally of the order of 10^2 mV, which is much higher than the overpotentials ($\sim 10^0$ mV) required to generate two-dimensional nuclei on different crystal planes. As a result, all types of two-dimensional nuclei may be generated equally. Therefore, it is hard to believe that the texture is created by the difference in the two-dimensional nucleation rate. Disagreement between this theory and experiments has also been found [6, 8–10].

A tentative Monte Carlo simulation model was developed by the present authors to simulate texture formation during electrodeposition. The model was developed based on the assumption that textural evolution during electrodeposition results from the minimization of the free energy of the system, in which the surface-energy anisotropy plays the most important role. The model also makes it possible to study inhibition effects of foreign species on textural evolution by investigating the effects of foreign species on textural evolution due to the effects of foreign species on the surface-energy anisotropy of the deposit.

The Monte Carlo technique for microstructure modelling was proposed by Anderson *et al.* [11–14]. Essential elements of their model consist in mapping the continuum microstructure on to a two-dimensional discrete lattice and defining interactions between the lattice sites, which are analogous to those in continuous systems. In their model, the lattice site is randomly selected to test its energy and orientation. A new state of this site is calculated according to the Metropolis algorithm [11–14]. This new state can be accepted only if the state-energy of the site decreases. As a result of the simulation, the whole system will reach a minimum-energy state. The Monte Carlo simulation technique has been used to simulate nucleation and grain growth during recrystallization, solidification and vapour deposition processes [15–18].

Electrodeposition is a nucleation and grain-growth process; the Monte Carlo simulation technique is, therefore, also applicable to modelling electrodeposit growth. It is possible to use this technique to simulate the texture evolution during electrodeposition processes. According to thermodynamics, a system always approaches a minimum free-energy state; it is, therefore, expected that the deposit growth selects a "path" which leads to a decrease in the free energy of the system, and this may result in a textured deposit. One may logically expect that the anisotropic grain growth (i.e. texture) could thus be modelled by taking into account the factors which are crystallographically anisotropic and related to the free energy of the system. This principle has been used in the present simulation.

2. Description of the Monte Carlo model

During electrodeposition, metal ions move to the cathode under the applied electric field. When approaching the cathode, the ions are discharged and then diffuse in the vicinity of the cathode surface until reaching favourable sites for accommodation. The evolution of microstructure and texture could be simulated by adding atoms to random locations on the cathode surface and allowing them to diffuse until reaching preferred sites. However, direct modelling this process is unrealistic, because it requires a large number of atoms to simulate the process, even at a very small area. Thus, the present approach is not an atomistic model but a quasi-continuum one, which accounts for the statistical nature of deposit growth.

In the present simulation approach, the following problems should be defined: (1) the representation of deposit microstructure; (2) the criterion for the deposit growth; (3) factors affecting the textural development; and (4) the parameter which controls the deposition rate.

2.1. Representation of the microstructure and texture of a deposit

In the simulation model, the microstructure at the cross-section of deposit is mapped on to a two-dimensional triangle lattice. The lattice site represents a certain volume, which is small enough, so that changes in the site's state can provide information about microstructure and texture evolution. Each site is assigned an integral number, P, to represent the orientation of the grain to which the site belongs. Initially, the lattice sites are not occupied, with their P values assigned at zero. As the deposit grows, the previously empty sites are occupied layer by layer. The occupation of a site is indicated by a change of its P value from zero to a positive integer. This process is modelled in the following way. First, nuclei are generated at the cathode surface. The lattice is then scanned layer by layer; during the scanning process, the site in each lattice layer is randomly selected. If $P = 0$, the site will be occupied and its P value will change to a positive integer. The value of this integer number is dependent on the change in local free energy. If $P > 0$, or the site has already been occupied, it will be skipped and no change will be made at this site.

In the model, a texture component is represented by its volume fraction, which is defined as the ratio of the number of the sites, which contribute to that texture component, to the total number of lattice sites. For a fibre texture component whose axis is normal to $\{h\,k\,l\}$ plane, its volume fraction is the ratio of the number of sites, which belong to the grains having their $\{h\,k\,l\}$ planes parallel to the deposit surface, to the total number of lattice sites.

2.2. Nucleation and grain growth

When electrodeposition commences, nucleation must occur. Such a situation is analogous to the nucleation from a supersaturated solution, or condensation from a supersaturated vapour [19]. When an ion enters the diffusion layer, it is dehydrated, discharged, and then diffuses and eventually joins other ad-atoms to form a nucleus. The more ad-atoms diffusing on the

cathode surface, the higher the nucleation probability. Because the density of ad-atoms is dependent on the flux of ions carried by the deposition current, the nucleation probability is, therefore, affected by the current density. The relationship between the nucleation probability and the current density can be expressed as [19, 20].

$$Fn \propto \exp[-\sigma/(RTi_c^2)] \quad (1)$$

where i_c, T and R are the current density, temperature, and gas constant, respectively. σ is a parameter proportional to the surface energy of the nucleus. From this formula one can see that a high current density results in a high nucleation rate. During electrodeposition, nucleation may also take place on the surface of a growing crystal. Compared to the grain growth, however, this type of nucleation is unfavoured, because it requires an activation energy to overcome the nucleation barrier which depends on the surface energy of the critical nucleus, but the grain growth does not.

According to thermodynamics, a system always approaches a minimum free-energy state. The deposit growth is, therefore, assumed to follow the minimization of the free energy of the system. As the deposit grows, the previously empty sites become occupied. The decision by which the P integer is selected for a new state of a site is determined by the change in energy of the site. The energy of a site is obtained by summing the interaction between the site and its neighbours. Because the site is not an atom but a network node, the interaction between the site and its neighbour site is, therefore, not the interaction between an atomic pair; but it can be, however, represented by a bond whose energy is proportional to the interfacial energy between this pair of sites. The energy of a site is expressed as

$$H = -J\sum_{nn}(\delta_{P_iP_j} - 1) + H_{hkl} \quad (2)$$

where J is one-half of the bond energy, or the interaction, between two neighbour sites. P_i represents the P value of site i, and $\delta_{P_iP_j}$ has the following value: $\delta_{P_iP_j} = 1$ if $P_i = P_j$ or $\delta_{P_iP_j} = 0$ if $P_i \neq P_j$.

The first term in Equation (2) represents the free energy of bonds, or the interaction, between the testing site and its neighbours. If a pair of sites have the same P values, there is no interaction between these two sites because there is no interface between them. Interaction only exists if the sites have different P values. More detail about the bond energy will be described later. In Equation 2, an additional term, H_{hkl}, is added to represent the energy anisotropy.

2.3. Factors responsible for texture development

When an ion arrives at the cathode surface, it loses its charge and diffuses along the cathode surface until it reaches a low-energy location, where it will be accommodated. The low-energy location is at the site, where the accommodation of the ad-atom causes the lowest increase in the free energy of the deposit; microsteps, kinks, and surface vacancies provide such favourable locations. In our simulation, however, the lattice site is not a crystal lattice site, but a site which represents a certain volume of the deposit. Whether or not a site is favourable for the deposit growth is, therefore, dependent on its average energy. The deposit will grow in such a way that it leads to a decrease in the energy of the system. Therefore, the factors which are crystallographically anisotropic and related to the free energy of the system will affect the texture development.

The surface-energy anisotropy is considered to be the most important factor responsible for texture formation. When arriving at a surface junction of two grains, an ad-atom tends to be accommodated by the grain which has a lower surface energy; this decreases the overall surface energy of the system. As a result, the surface junction will move towards the grain having the higher surface energy, and its neighbour would therefore grow preferentially. This competition can be realized in the Monte Carlo simulation. When a lattice site in the junction of two grains is occupied, its orientation is determined by its state-energy. Because this site is located at the deposit surface and neighbours with unoccupied sites, the interaction between the site and its empty neighbour sites, therefore, depends on the surface energy, and the surface energy anisotropy will affect the selection of the P value for this site. The chosen P value should lead to a decrease in the surface energy, and therefore, the grain having low surface energy would grow preferentially.

2.4. Current density: the parameter controlling the deposition rate

In the Monte Carlo simulation, the current density is used as a parameter to control the deposition rate, because it relates to the charge transfer and mass transfer, and affects the deposition rate as described by Faraday's law [21, 22]

$$\frac{dh}{dt} = \frac{h}{t} = \frac{i_c \omega E_{el}}{60\rho} \quad (3)$$

where h is the thickness of the deposit, and E_{el} is the electrochemical equivalent of the deposited metal. t, ρ and i_c are the deposition time, density of the deposit, and the current density, respectively. ω is the current efficiency. The deposition rate is proportional to the current density. Using the current density to control the process is also due to the fact that the current density is related to the microstructure of the deposit, as the nucleation probability is affected by the current density. The grain size of the deposit is, therefore, influenced by the current density. The current density also affects the strength of the texture of the deposit. It is known that at a high current density, deposits may grow in the form of powder [19] without any texture; but at a lower current, the same deposit can be strongly textured.

There are some difficulties, however, in using the current density directly as an input in the simulation. The current density should be converted into a parameter which can be simulated, To do this, we define

the scanning of one lattice layer with 200 iterations to be one Monte Carlo Step (MCS). Because each iteration takes a certain time, one MCS thus corresponds to a time interval. The deposition rate can, therefore, be modelled by using different number, n, of MCSs in scanning one layer; i.e. the necessary time, Δt, to deposit an increment of the deposit thickness, Δh, can be replaced by n(MCS)

$$\Delta h/\Delta t \propto \Delta h/(\mathrm{MCS}) \tag{4}$$

The deposition rate is lower if the number of MCSs, n, is higher. Because the deposition rate is proportional to the current density (see Equation 3), the current density can be represented as a function of n for the purpose of simulation

$$\begin{aligned} i_c &\propto \Delta h/\Delta t \\ &\propto \Delta h/n(\mathrm{MCS}) \\ &\propto 1/n \end{aligned} \tag{5}$$

The effect of current density on the texture and microstructure of the deposit can thus be modelled by using a different number, n, of Monte Carlo steps for scanning each lattice layer.

2.5. The simulation procedure

The input for the simulation includes the number of MCSs used to scan one lattice layer, and anisotropy factors such as the surface-energy anisotropy. The anisotropy factors determine the competition between different crystallographic planes, and are therefore responsible for texture development.

Nuclei are initially generated at the substrate surface. The lattice is then scanned layer by layer, from bottom to top. The deposition rate is controlled by the number of MCSs used in scanning one layer. During scanning a lattice layer, the site is randomly selected for testing. If its P value is equal to zero, this site will be occupied, and its orientation will depend upon the calculated energy change of the site. If the tested site already has a non-zero P value, the calculation will not be continued.

Initially energy, H_0, of the selected site is calculated using a rewritten form of Equation 2

$$H = -J\sum(\delta_{P_iP_j} - 1) + J'\sum{}'H^s_{hkl} + H_{uvw} \tag{6}$$

For a pair of occupied sites with different orientations, the bond energy corresponds to the grain boundary energy, γ_{gb}; if the bond connects an occupied site and an unoccupied site, its energy corresponds to the surface energy, γ_s. Therefore, the bond energy, $2J$, has different values for different bonds. If the value of the "grain-boundary bond" is defined as $2J$, the "surface bond", $2J'$, is then equal to $2J\,(\gamma_s/\gamma_{gb})$. In Equation 6, H^s_{hkl} is a modification term, which makes the "surface bond" energy crystallographically anisotropic. This anisotropy term represents the difference between the surface energy of the $\{h\,k\,l\}$ plane and the average surface energy, γ_s. Sum $\sum$ is taken over the six nearest neighbour sites, while $\sum'$ is taken over only those sites which are connected to the testing site by "surface bonds". To simplify the energy calculation, an average value of the grain-boundary energy is used. It is known that the most popular grain boundaries in polycrystalline materials are high-angle boundaries characterized by large misorientation, and have a high value of boundary energy. The high-angle boundaries are structurally complicated and irregular. Their energies are usually represented using an average value which is determined experimentally. In this simulation model, the concept of average GB energy is adopted. To summarize, in the simulation, a "grain-boundary bond" has an energy equal to $2J$, and a "surface bond" has an energy equal to $2J'\ (1 + H^s_{hkl}) = 2J\,(\gamma_s/\gamma_{gb})(1 + H^s_{hkl})$. The term, H_{uvw}, is used to represent effect of other possible anisotropic energy contributions. For example, if the deposition is performed in a magnetic field, a magnetization energy term, H^m_{uvw}, may be added, e.g. $H_{uvw} = H^m_{uvw}$. The magnetization energy term, H^m_{uvw}, is defined only for occupied sites. The notation, $u\,v\,w$, represents the orientation of the site which is parallel to the magnetic field. This term accounts for the anisotropic effect of magnetic field on deposit texture.

After H_0 is calculated, the P value of the testing site is changed from zero to a P value of its nearest neighbours, and a trial energy, H_n, is calculated. P values of all nearest neighbours are used in the same way to test which site configuration has the lowest energy. The minimum H_n is then chosen, and the corresponding P integer is assigned to the testing site. If $\Delta H = H_n - H_0 < 0$, this change in P value is accepted. H_n is, however, sometimes larger than H_0, and this case often occurs at grain boundaries, where the nucleation rate is usually high. Therefore, if $\Delta H \geqslant 0$, a randomly oriented nucleus is generated in the probability [19, 20]

$$F \propto \exp(-\sigma/RTi_c^2) = \exp(-\sigma' n^2/RT) \tag{7}$$

where σ' is a constant.

The output of the simulation will provide the information about the texture, grain size, and grain shape of the deposit.

3. Surface-energy anisotropy of iron

3.1. Surface-energy anisotropy of iron

As proposed, the surface-energy anisotropy plays the most important role in textural evolution. The surface-energy anisotropy is therefore a key input for the simulation, and it needs to be calculated before starting the simulation. In this study, iron was chosen as an example, with the emphasis on investigating hydrogen effects on texture formation in iron deposits. A pair-potential method was employed for the calculation, and the Lennard-Jones [23] potential was used. A $2.86 \times 2.86 \times 2.86\ \mathrm{nm}^3$ cubic cell containing 2000 iron atoms was constructed, followed by the relaxation of surface atoms. During the relaxation process, each of the surface atoms was allowed to move randomly by a short distance. If the old configuration energy is defined as E_1, and the new configuration

energy after the atomic shift is defined as E_2, each move is accepted with a probability $P = \exp[-(E_2 - E_1)/KT]$; where K is Boltzmann's constant and T is temperature. Note that if $E_2 < E_1$, the probability of such a move is always larger than unity, and therefore, such a move is then always accepted. The surface energy of a crystallographic plane $(h\,k\,l)$ is defined as the difference in configuration energy between the surface layer and the middle layer, parallel to the $(h\,k\,l)$ plane of the crystal. In order to calculate the surface energy, the energy of the surface layer (0.3 nm thick) was calculated and compared to that of the central layer. The difference between these two energies gives the surface energy of the $(h\,k\,l)$ plane. Choosing the layer of 0.3 nm thick for the surface energy calculation was justified by the fact that the interaction between a pair of atoms declines as the distance between them increases, and that the nearest neighbours contribute to approximately 90% of the energy of the system. So, in this calculation, the calculated layers are 0.3 nm thick, and this distance covers the nearest and second nearest neighbours (the distances to the nearest and second nearest neighbours are 0.248 and 0.287 nm, respectively). Surface energies of a number of low-index iron crystal planes were calculated, and the result is presented in Fig. 1. Most of these planes correspond to the fibre textures, which were reported to exist in iron electrodeposits.

3.2. The effect of hydrogen adsorption on iron surface energy

Metal deposit is often accompanied by a simultaneous hydrogen co-deposition [21, 24]. When the hydrogen co-deposition takes place, it affects the surface energy of the deposit, and the surface energy is lowered by the absorbed hydrogen. For example, the surface energy of iron can be lowered by approximately 800 erg cm^{-2}, when adsorbed hydrogen reaches 0.5 cm^3/100 g [25]. Lowering the surface-energy is different for different crystallographic planes because of their different adsorption abilities [1]. It was demonstrated, by means of a quantum-mechanical calculation [26], that the greater the distance between adjacent metal atoms, the lower is the activation energy for hydrogen adsorption, i.e. surface energies of loosely packed planes decrease more rapidly than closely packed planes.

Surface-energy changes with the hydrogen adsorption were estimated to investigate how hydrogen affects the texture evolution. The hydrogen effect on iron surface energy was evaluated in the following way: different concentrations of hydrogen atoms were randomly distributed in close vicinity to the iron crystallographic plane under investigation. The hydrogen and iron atoms in the surface region were then relaxed, and after the relaxation, the configuration energy of a surface layer (0.3 nm thick) of the iron crystal was calculated. The energy difference between the relaxed surface layer and a non-relaxed central layer of equal thickness gave the surface energy, which was influenced by adsorbed hydrogen.

Fig. 2 illustrates the effect of hydrogen on the surface energies of various crystallographic planes. One may see that the iron surface energy is lowered as the hydrogen concentration increases, and that the lowering rates for different planes are different. It is, therefore, expected that, as the hydrogen co-deposition increases, the texture will change from one type to another, due to the changes in the surface-energy anisotropy.

4. Simulation results and discussion

4.1. Texture of iron deposits free from adsorption of foreign species

The evolution of six fibre textures in iron deposits, reported in the literature [7, 27–30], were simulated. Axis orientations of these fibre textures are ⟨1 1 0⟩, ⟨1 1 1⟩, ⟨1 0 0⟩, ⟨2 1 1⟩, ⟨3 1 0⟩, and ⟨3 1 1⟩. Three deposition rates were used in the simulation. The texture of the simulated deposit, containing the six components, is illustrated in Fig. 3. It is demonstrated that the components, which correspond to lower surface energies, have higher volume fractions, and as such, the ⟨1 1 0⟩ fibre texture is the strongest and it dominates the texture of the deposit. One may also see that the ⟨1 1 0⟩ texture becomes less pronounced as

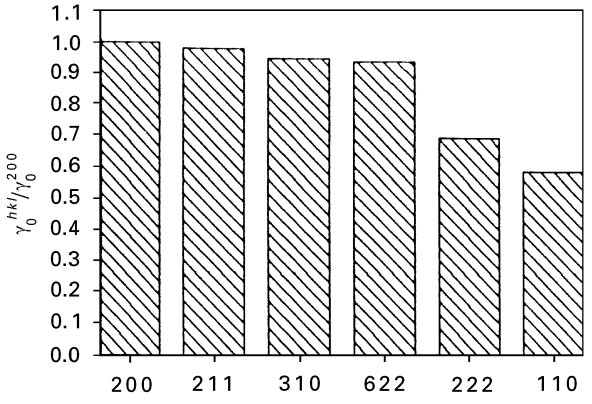

Figure 1 Calculated surface energies of iron (normalized). The Lennard–Jones potential was used in the calculation. γ_0^{200} is the surface energy of the (2 0 0) plane free from hydrogen adsorption.

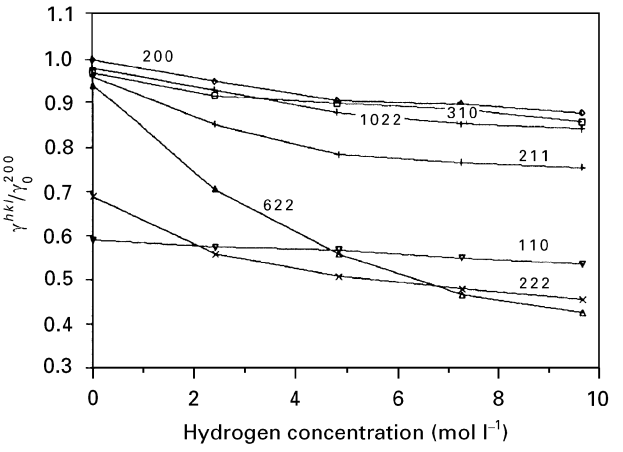

Figure 2 The effect of hydrogen on the surface energies of iron of various crystallographic planes. γ_0^{200} is the surface energy of the (2 0 0) plane free from hydrogen adsorption.

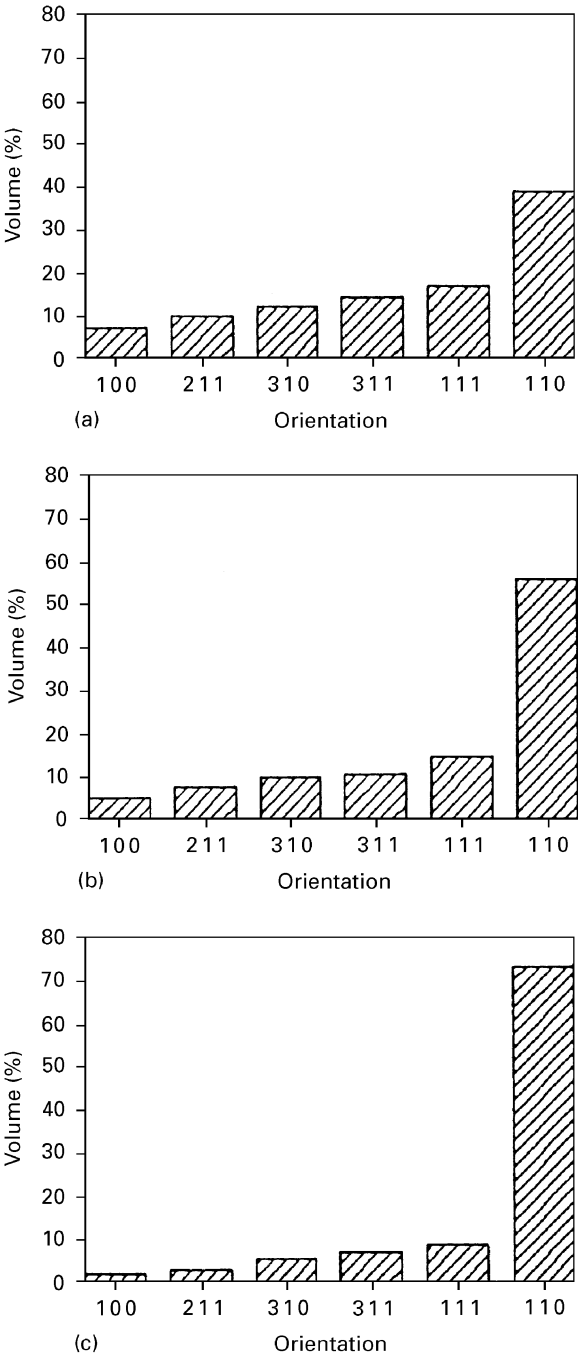

Figure 3 Volume fraction of the six texture components obtained at deposition rates of (a) $n = 6$, (b) $n = 13$, (c) $n = 21$.

the deposition rate increases. This is attributed to an increase in nucleation rate when the deposition rate increases; the increased nucleation does not favour the selective grain growth, and is, therefore, responsible for lowering the texture strength as the deposition rate increases.

4.2. Texture variation caused by hydrogen co-deposition

The main task of this work is to investigate effects of hydrogen adsorption on texture formation in iron deposits. The texture of a deposit may change when hydrogen co-deposition takes place. This is a result of lowering the metal's surface energy by hydrogen adsorption. It has been demonstrated that the surface-energy anisotropy of iron changes as the hydrogen concentration increases (Fig. 2). The hydrogen co-deposition is dependent on the current density, or potential, bath temperature, and the pH value of the electrolyte [21, 24]. One may, therefore, expect that the deposit texture will change with changes in the deposition conditions.

The texture variation of iron deposit with hydrogen adsorption was simulated. Surface energies of various iron planes affected by hydrogen are presented in Fig. 2. It can be seen that the $\{1\,1\,0\}$ plane has the lowest surface energy, and that by increasing the hydrogen concentration, the lowest surface-energy state is observed at the $\{1\,1\,1\}$ plane, and then the $\{3\,1\,1\}$ plane, respectively. Based on these results, texture formation at different hydrogen concentrations was simulated. The simulation demonstrates that by increasing hydrogen concentration, the iron deposit changes its texture from $\langle 1\,1\,0\rangle$, through $\langle 1\,1\,1\rangle$, to $\langle 3\,1\,1\rangle$ fibre texture (Fig. 4). This change in texture is caused by varying the iron surface-energy anisotropy through hydrogen adsorption.

4.3. The effect of current density, bath temperature, and the bath pH value on texture formation

Hydrogen co-deposition is strongly influenced by the current density, bath pH value, and the bath temperature. The present simulation has illustrated how texture changes with hydrogen adsorption, and this may explain the diversity in texture of iron deposits obtained in different deposition conditions, in which the hydrogen co-deposition may play the major role.

At the surface of the cathode, the content of adsorbed hydrogen is proportional to the hydrogen concentration in the vicinity of the cathode surface, or to the hydrogen coverage θ [31], which increases as the hydrogen overpotential increases (i.e. is more negative) [31, 32]

$$\theta \propto \exp(-\kappa\eta_H/RT) \qquad \eta_H < 0 \tag{8}$$

where κ is a constant, and η_H is the hydrogen overpotential. The hydrogen overpotential is the difference between the cathode potential, E, and the hydrogen equilibrium potential, E_H^{eq} [24]

$$\eta_H = E - E_H^{eq} = E + \frac{RT}{F}\,\mathrm{pH} \tag{9}$$

where F and R are the Faraday's constant and gas constant, respectively. From Equations 8 and 9 we see that the hydrogen co-deposition is affected by the bath temperature, the pH value of the bath, and the deposition potential which is related to the current density. Because these parameters can be controlled during electro-deposition, controlling the texture of the deposit becomes possible.

4.3.1. The effect of current density

Increasing the current density corresponds to increasing the cathode potential (i.e. more negative), and this

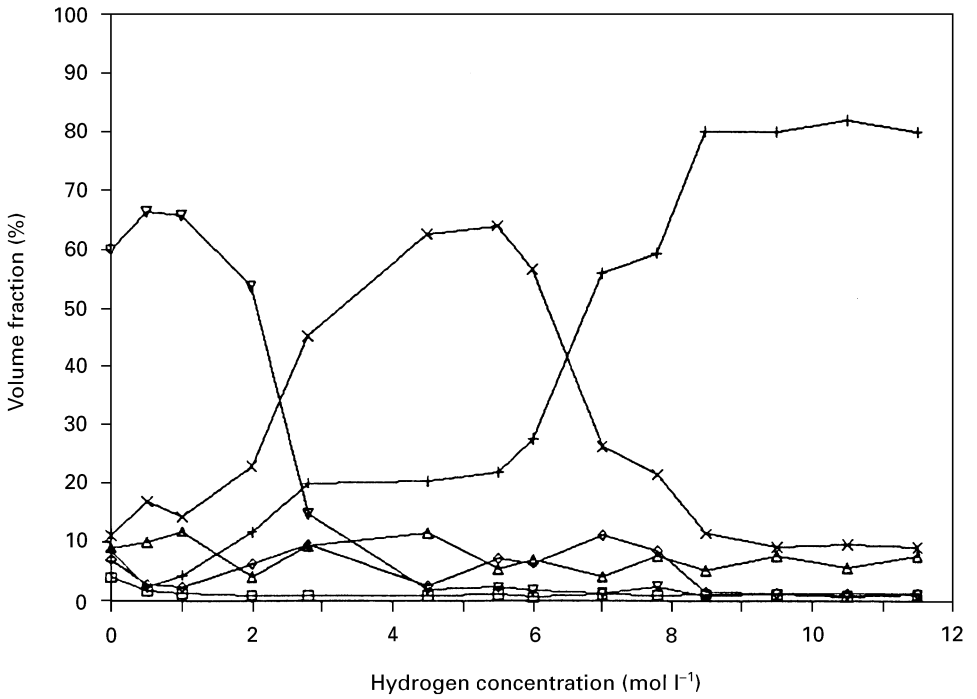

Figure 4 Changes in the axis of the iron deposit's fibre texture from ⟨1 1 0⟩, through ⟨1 1 1⟩, to ⟨3 1 1⟩ type with an increase in the content of adsorbed hydrogen. (□) 1 0 0, (+) 3 1 1, (◇) 2 1 1, (△) 3 1 0, (×) 1 1 1, (▽) 1 1 0.

leads to an increase in the hydrogen overpotential (see Equation 9). For example, for iron deposition, the absolute value of the hydrogen overpotential is 0.40 V at 0.1 A dm^{-2}, 0.53 V at 1 A dm^{-2}, and 0.64 V at 10 A dm^{-2} [21]. Therefore, increasing the current density will increase the content of the adsorbed hydrogen. As a result, the axis of fibre texture will change in the following order: ⟨1 1 0⟩ → ⟨1 1 1⟩ → ⟨3 1 1⟩.

4.3.2. The effects of pH value

As seen from Equations 8 and 9, the hydrogen overpotential decreases (becomes less negative) with an increase in the pH value of the bath. This leads to a decrease in the hydrogen coverage, θ. As a result, less hydrogen is adsorbed by the cathode, and the fibre texture of the iron deposit will, therefore, change its axis in the following order: ⟨3 1 1⟩ → ⟨1 1 1⟩ → ⟨1 1 0⟩.

4.3.3. The effect of bath temperature

According to Equations 8 and 9, increasing the temperature, similar to increasing the pH value, reduces the hydrogen adsorption. The temperature effect is, however, more complicated, and it involves several factors: (1) a decrease in the absolute value of the hydrogen overpotential; (2) an increase in temperature as a variable in Equation (8); and (3) an increase in hydrogen desorption. As a result of increasing the bath temperature, the fibre texture changes in the order: ⟨3 1 1⟩ → ⟨1 1 1⟩ → ⟨1 1 0⟩.

It should be pointed out that the present simulation only provides qualitative information, because the hydrogen adsorption is a complex process, and the amount of adsorbed hydrogen is difficult to calculate.

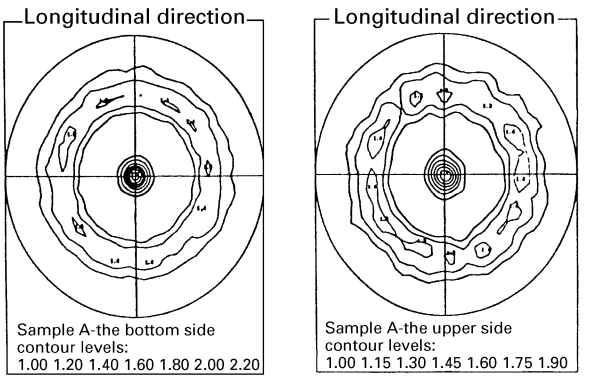

Figure 5 Pole figures measured at two sides of an iron electrodeposit with thickness equal to 0.28 mm. A ⟨1 1 0⟩ fibre texture was formed in the deposit.

Nevertheless, the tendency of texture variation can be predicted from the Monte Carlo simulation.

5. Experimental observation

Relevant experiments were conducted to corroborate the simulation results. In particular, effects of the current density, bath temperature, and the pH value of the bath on texture formation were investigated and compared with the simulation prediction.

The electrodeposition set includes a 300 ml glass container, a heating bath circulator, a magnetic stirrer, and a d.c. power supply. The wall of the glass container is double-layered, and contains water from the heating bath circulator, thereby controlling the bath temperature. The magnetic stirrer is used to enhance

the convection of the solution for efficient mass transfer. The cathode and anode were made of Armco iron, and they had sizes of $24 \times 14 \times 4$ and $25 \times 25 \times 4$ mm^3, respectively. The distance between the cathode and anode was approximately 27 mm. The electrolyte used for the iron deposition consisted of 400 g l^{-1} ferrous chloride and 80 g l^{-1} calcium chloride. The calcium chloride in the electrolyte was used to increase cathodic current efficiency, reduce internal tensile stress, and to prevent the oxidation of the ferrous ions into ferric

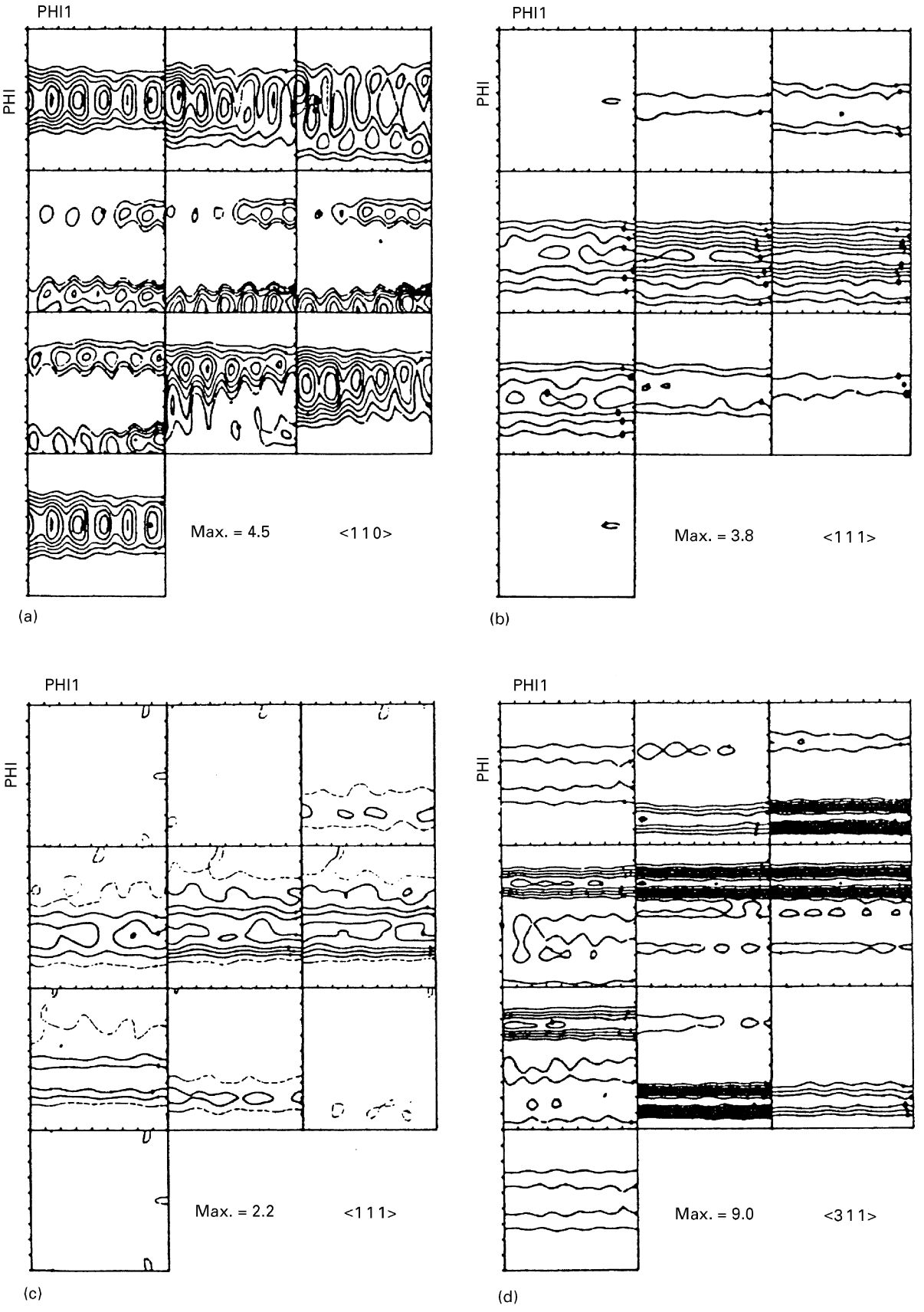

Figure 6 The current density effect on the texture of the iron deposit at 70 °C, pH = 1.7: (a) $i = 4.5$ A dm^{-2}, (b) $i = 30$ A dm^{-2}, (c) $i = 75$ A dm^{-2}, (d) $i = 150$ A dm^{-2}.

ions when the bath is idle. In order to study the effect of the pH value of the bath on texture formation, hydrochloric acid was used to control the pH value. One or two drops of the hydrochloric acid can decrease the pH value dramatically. The pH value of the bath was determined using Alkacid pH paper with an accuracy of ± 0.25. The texture of the electrodeposits was measured using a Siemens X-ray

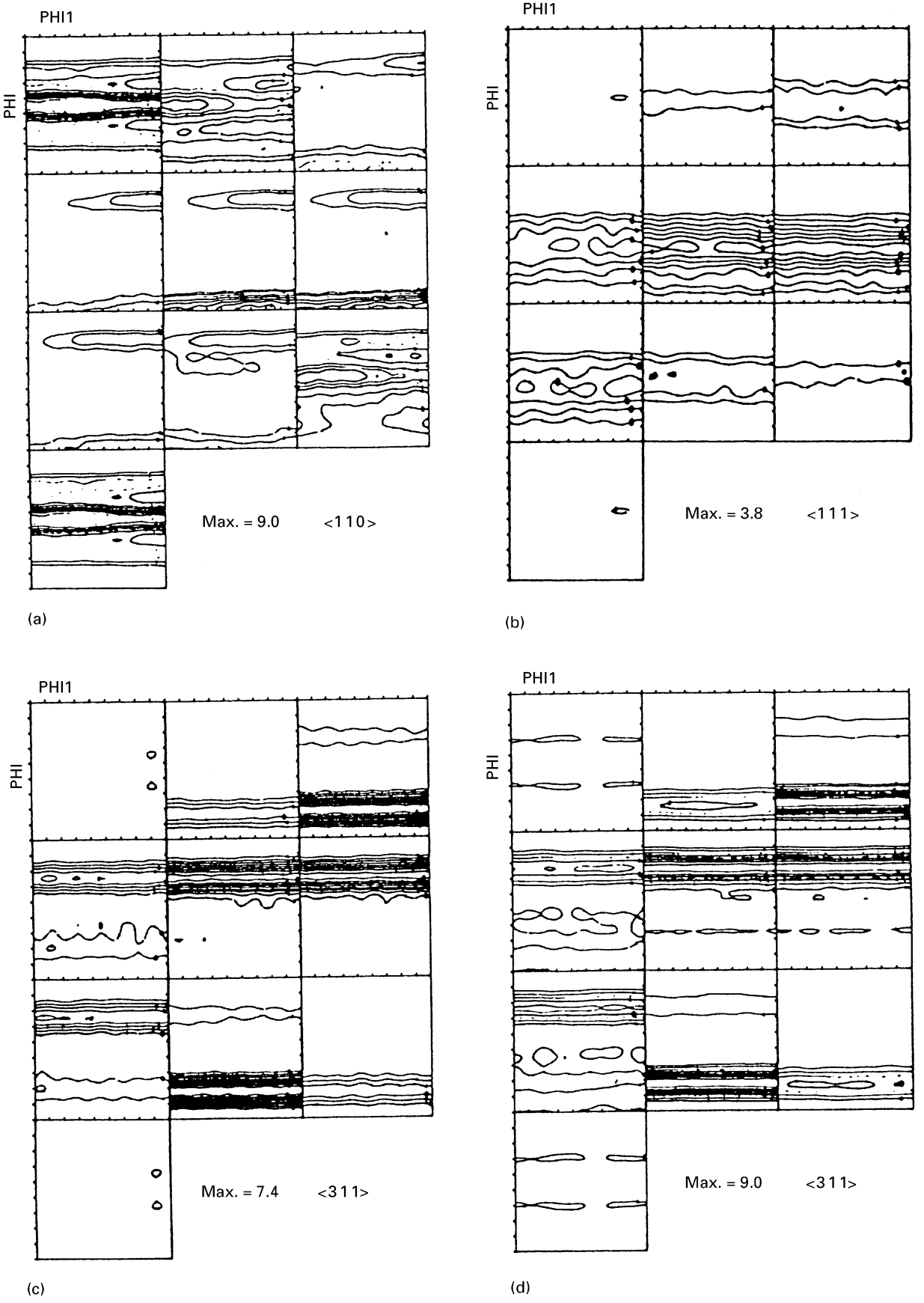

Figure 7 The temperature effect on the texture of the iron deposit at $i = 30\,A\,dm^{-2}$, pH = 1.7: (a) $T = 90\,^{\circ}C$, (b) $T = 70\,^{\circ}C$, (c) $T = 50\,^{\circ}C$, (d) $T = 25\,^{\circ}C$.

diffractometer with CuK_α radiation. Microstructure at the cross-section of the iron electrodeposits was observed using an optical microscope; specimens for the microstructure observation were mechanically polished, and then etched using an etchant which consisted of 10% HNO_3 and 90% alcohol by volume.

6. Experimental results

Iron deposition was performed under the following condition: $T = 90°C$, $i_c = 30\ A\,dm^{-2}$, pH = 1.7. Under such a condition, high quality, and bright iron deposits were obtained. It was determined that under such a deposition condition, the deposit exhibits a $\langle 1\,1\,0 \rangle$ fibre texture as illustrated in Fig. 5.

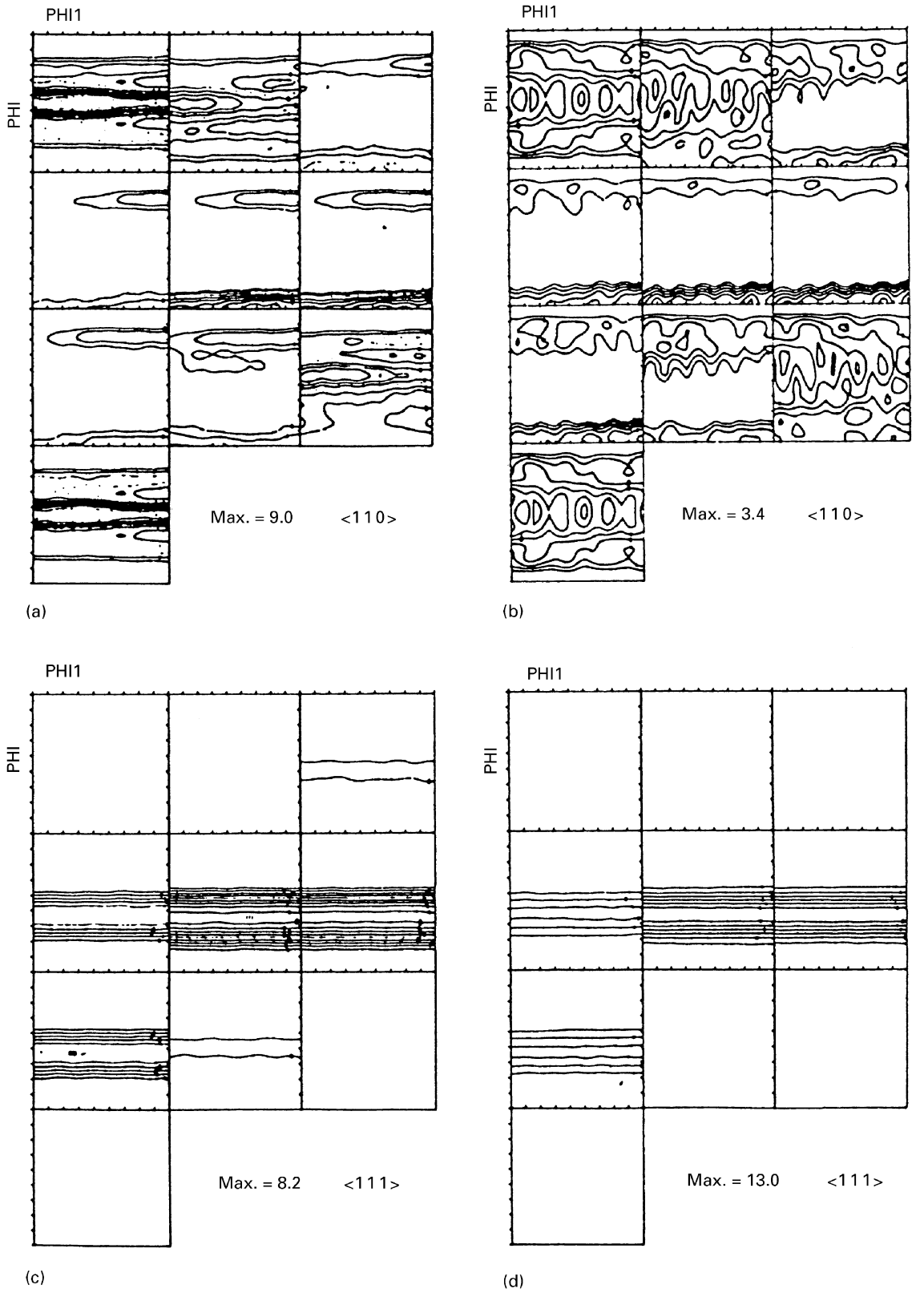

Figure 8 The effect of bath pH on the texture of the iron deposit at 90 °C, $i = 30\ A\,dm^{-2}$: (a) pH = 1.7, (b) pH = 1.0, (c) pH = 0.5, (d) pH = 0.

6.1. The texture variation with the deposition conditions

6.1.1. The effect of current density

Current density is often used to control electrodeposition because it relates directly to the deposition rate, or the weight of the deposited substance. In order to investigate the current density effect on texture formation, iron electrodeposits were made under different current densities, and their textures were measured. The deposition was carried out at 70 °C, and the pH value of the bath was 1.7. Fig. 6 illustrates the orientation distribution functions (ODFs) of these deposits. It is demonstrated that three types of fibre texture developed in the iron electrodeposits at different current densities: at low current density the iron deposit has a ⟨1 1 0⟩ fibre texture, and the texture changes to a ⟨1 1 1⟩ fibre texture, and then to a ⟨3 1 1⟩ fibre texture when the current density is increased.

6.1.2. The effect of bath temperature

In order to investigate the effect of bath temperature on texture formation, textures of iron deposits formed at 30 A dm^{-2} and pH = 1.7, but at different bath temperatures, were measured. ODFs of these deposits are illustrated in Fig. 7. The above-mentioned three types of fibre texture were observed again at different bath temperatures: the texture of the iron deposit changed from a ⟨1 1 0⟩ fibre, through a ⟨1 1 1⟩ fibre, to a ⟨3 1 1⟩ fibre texture, as the bath temperature decreased from 90 °C to 25 °C.

6.1.3. The effect of the bath pH value

The texture of the iron deposit shows a strong response to changes in the bath pH level. Textural evolutions at pH of 1.7, 1.0, 0.5, and 0 were measured, respectively. The current density and bath temperature for the deposition were 30 A dm^{-2} and 90 °C, respectively. Fig. 8 illustrates the results of the texture measurement. At pH = 1.7, the deposit showed a ⟨1 1 0⟩ fibre texture, while decreasing the pH value made the ⟨1 1 0⟩ fibre texture weaker, and it was eventually replaced by the ⟨1 1 1⟩ fibre texture as the pH value approached zero.

It was noted that ⟨3 1 1⟩ fibre texture was not observed at 90 °C, even as the pH was decreased to zero. The absence of ⟨3 1 1⟩ texture may be attributed to the high bath temperature. Indeed, the ⟨3 1 1⟩ texture appeared at lower temperatures. Fig. 9 presents the ODF of iron deposit formed at the same current density but at 70 °C with a pH value of zero. It is illustrated that in this case, the ⟨3 1 1⟩ fibre texture was formed.

Compared with the simulation prediction, a positive correlation between the simulation and experimental observation was found.

7. Conclusion

The texture formation during iron electrodeposition and hydrogen effects on textural variation were studied using a Monte Carlo model. It was demonstrated that the texture growth resulted from minimizing the free energy of the system, and that the surface-energy anisotropy played an important role in the formation of fibre texture. The fibre texture was changed by varying the current density, the pH value, or temperature of the bath. The changes in texture with the deposition condition could be attributed to the hydrogen co-deposition which may modify the surface-energy anisotropy of the deposit. The mechanism of textural variation with hydrogen co-deposition through changes in the deposition condition has been discussed. Relevant experiments were conducted to corroborate the simulation. A qualitative agreement between the simulation prediction and the experiments was found.

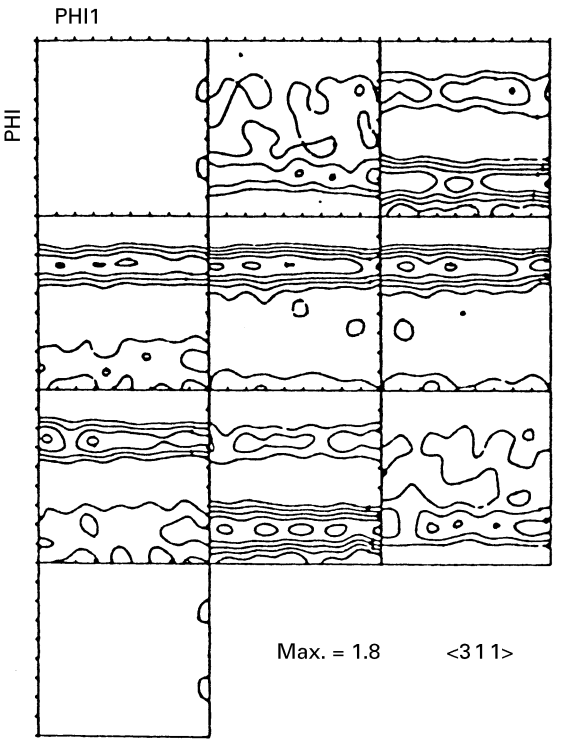

Figure 9 The ODF of iron deposited at 70 °C, i = 30 A dm^{-2}, and pH = 0.

References

1. A. K. N. REDDY, *J. Electroanal. Chem.* **6** (1963) 141.
2. N. A. PANGAROV, *ibid.* **9** (1965) 70.
3. A. N. BARABOSHKIN, Z. S. MARTEM'YANOVA, S. V. PLAKSIN and N. O. ESINA, *Élektrohimiya* **13** (1977) 1807.
4. *Idem*, *ibid.* **14** (1978) 9.
5. J. AMBLARD and M. FROMENT, *Farad. Symp. Chem. Soc.* (12) (1978) 136.
6. G. C. YE and D. N. LEE, *Plating Surf. Finish. A* vol. 68 (1981) 60.
7. N. A. PANGAROV and S. D. VITKOVA, *Electrochem. Acta* **11** (1966) 1719.
8. I. EPELBOIN, M. FROMENT and G. MAURIN, *Plating* **56** (1969) 1356.
9. I. A. MENZIES and C. X. NG, *Trans. Inst. Met. Fin.* **47** (1956) 156.
10. J. R. PARK and D. N. LEE, *J. Korean Inst. Metals* **12** (1976) 243.
11. M. P. ANDERSON, D. J. SROLOVITZ, G. S. GREST and P. S. SAHNI, *Acta Metall.* **32** (1984) 783.

12. D. J. SROLOVITZ, M. P. ANDERSON, P. S. SAHNI and G. S. GREST, *ibid.* **32** (1984) 793.
13. D. J. SROLOVITZ, M. P. ANDERSON, G. S. GREST and P. S. SAHNI, *ibid.* **32** (1984) 1429.
14. G. S. GREST, D. J. SROLOVITZ and M. P. ANDERSON, *ibid.* **33** (1985) 509.
15. D. J. SROLOVITZ, G. S. GREST and M. P. ANDERSON, *ibid.* **34** (1986) 1833.
16. D. J. SROLOVITZ, G. S. GREST, M. P. ANDERSON and A. D. ROLLETT, *ibid.* **36** (1988) 2115.
17. D. J. SROLOVITZ, *J. Vac. Sci. Technol.* **A4** (1986) 2925.
18. J. A. SPITTLE and S. G. R. BROWN, *J. Mater. Sci.* **23** (1989) 1777.
19. RENÉ WINAND, "Fundamentals and Practice of Aqueous Electrometallurgy" (short course) (The Metallurgical Society of CIM, Montreal, PQ, Canada 1990), p.7.
20. J. O'M. BOCKRIS and G. A. RAZUMNEY, "Fundamental Aspects of Electrocrystallization" (Plenum Press, New York, 1967).
21. E. RAUB and K. MÜLLER, "Fundamentals of Metal Deposition" (Elsevier, Amsterdam, 1967).
22. D. R. CROW, "Principles and Applications of Electrochemistry" (Chapman and Hall, London, 1974).
23. T. HALICIO ĞLU and G. M. POUND, *Phys. Status Solidi* (*a*) **30** (1975) 619.
24. N. V. PARTHASARADHY, "Practical Electroplating Handbook" (Prentice-Hall, Englewood Cliffs, NJ, 1989).
25. N. J. PETCH, *Philos. Mag.* **1** (1956) 331.
26. G. OKAMOTO, J. HORIUTI and K.HIROTA, *Sci. Papers Inst. Chem. Res.* (*Tokyo*) **29** (1936) 223.
27. R. GLOCKER and E. KAUPP, *Z. Physik* **24** (1924) 121.
28. R. M. BOZORTH, *Phys. Rev.* **26** (1925) 390.
29. C. B. BARRETT and T. B. MASSALSKI, "Structure of Metals", 3rd Edn (Pergamon Press, Elmsford, New York, 1980).
30. N. V. KOTEL 'NIKOV, *Fiz. Metal. Metalloved* **6** (1958) 222.
31. R. N. IYER, H. W. PICKERING and M. ZAMANZADEH, *J. Electrochem. Soc.* **136** (1989) 2463.
32. C. D. KIM and B. E. WILDE, *ibid.* **118** (1971) 202.

Received 13 November 1995
and accepted 10 February 1997